

UNDERSTANDING LINEAR AND RADIAL FLOW FOR IN-PLANE PERMEABILITY DETERMINATION IN THE ACCURACY OF LCM SIMULATION

Joana M. Malheiro¹ and Paulo Antunes¹

¹ Advanced Manufacturing Processes (Composites), PIEP – Innovation in Polymer Engineering, University of Minho, Campus de Azurém, 4800-048 Guimarães – Portugal, www.piep.pt, joana.malheiro@piep.pt and paulo.antunes@piep.pt

Keywords: in-plane permeability, radial and linear flow, continuous fibre reinforcement, Liquid Composite Moulding, simulation of impregnation process

ABSTRACT

The prediction and optimization of the impregnation process by numerical approaches have been widely used, to avoid expensive experimental setups and prototypes. Although the fluid flow within a fibrous reinforcement has been extensively studied, it is very difficult to model, in particular, because the porous media is difficult to characterize. The most important parameter to describe a porous media is permeability (K), which is not an intrinsic property of the fibrous reinforcing material. The accurate numerical modelling of the LCM manufacturing process of composite materials, implies the determination of the exact permeability tensor of a specific reinforcement. However, the same method leads to different results. In this study, linear and radial flow methods, followed by different data analysis, were used to determine the in-plane permeability of a fibre reinforcement. The permeability values calculated are then used in the numerical simulation of the impregnation process. The correlations established between experimental and simulation results, are then considered, first, to access the accuracy of the different approaches and, second, to establish which approach is the most appropriate to determine the permeability tensor for the accurate simulation of complex geometries.

1 INTRODUCTION

In every Liquid Composite Moulding (LCM) manufacturing process of fibre reinforced polymer composites (FRPC), dry continuous fibre reinforcements are placed in a mould and impregnated with a liquid polymer matrix material [1,2]. Effective impregnation of the dry reinforcements plays an important role in the quality of the final part, as unsaturated zones directly affect its mechanical properties. The impregnation process comprises: flow of viscous fluids (the liquid matrix) in porous media (the fibrous reinforcing structure), and interactions between them (e.g., wetting, swelling). Although these are extensively studied and well understood phenomena [3], they are very difficult to model, due to their mathematical complex relations, and cannot be solved analytically, except for particular flow problems. The flow of viscous fluids in fibrous media, for example, with typical Reynolds number (Re) in the order of 10^{-1} (i.e., fluid viscous forces are dominant and inertial effects can be neglected), can be described by Darcy's law [3-5]:

$$u = \frac{K}{\mu}(\Delta p - \rho g) \quad (1)$$

which relates the volume average fluid velocity (u), driving pressure (p) and gravity (g) to the permeability (K) and, the dynamic viscosity (μ) and density (ρ) of the fluid [4]. Due to its mathematical simplicity and reasonable accuracy, Darcy's law is the most applied equation to describe composite processing governing phenomena.

According to Darcy's law (1), the flow in porous media depends on the fluid properties, the flow conditions and the porous media architecture. The fluid properties and behaviour can be characterized adequately by density, viscosity and surface tension, while pressure and temperature are among the main factors driving flow conditions. The porous medium, is described by [3]: porosity (ϕ) and permeability (K). Porosity (ϕ), is the fraction of the bulk volume of the porous material that is occupied by pore or

void space [3]. Determines the amount of space which can be filled with fluid:

$$\phi = 1 - V_f \quad (2)$$

where, V_f is the fibre volume fraction. Permeability (K), is the conductivity of the porous media by a fluid, but is independent of the fluid properties and flow mechanism [3]. Also, permeability of a fibrous reinforcements is not an intrinsic property of the material, but a property which varies with different parameters, such as [6,7]: volume fraction, compression, material architecture (yarn structure, different fabrics, mats, knits, stacking, orientation, etc.), geometry (deformation or drape), surface properties, porosity, intra-yarn properties and fibre swelling.

The accurate numerical modelling of the LCM manufacturing process, implies the determination of the exact permeability tensor of a specific reinforcement. However, the state of the art of flow simulation is far more advanced than the capability in measuring permeability [4,5,8]. In fact, a number of different non-standard permeability measurement methods exist, but they lead to different results for the same material [8-10]

2 MEASUREMENT OF PERMEABILITY

Permeability describes the ease with which a fluid is transported through the tortuous void space, is expressed as m^2 and can be determined by Darcy's Law [11]. As an indirect method, the determination of permeability relies on the analytical analysis of the flow. The fibrous structure is, in most cases, assumed to be homogeneous (constant permeability), with direction dependence, therefore, expressed by a symmetric second order tensor \mathbf{K} , defined by the three principal components of the orthogonal coordinate system:

$$\mathbf{K} = \begin{pmatrix} K_{xx} & K_{yx} & K_{zx} \\ K_{xy} & K_{yy} & K_{zy} \\ K_{xz} & K_{yz} & K_{zz} \end{pmatrix} = \begin{pmatrix} K_1 & 0 & 0 \\ 0 & K_2 & 0 \\ 0 & 0 & K_3 \end{pmatrix} \quad (3)$$

Two of the principal axes (K_1 and K_2) are assumed to lie in the fabric plane due to the layer structure of the reinforcement material (in-plane permeabilities), and the third axis (K_3) is perpendicular to the fabric layer (out-of-plane permeability). It should be noted that K_1 and K_2 may not necessarily correspond to fibre direction in the fabric structure [12]. However, this assumption simplifies the analysis but is not realistic due to porous media structure variability [13]. In fact, few investigations have shown that the skew components should be taken in account and the six components of the permeability tensor should be known [13,14]. Yun et al [13] showed that transverse flow depends on the in-plane permeability components, and Okonkwo et al. [14] suggested that the skew component K_{xy} is essential to determine the accurate in-plane permeability principal components.

In order to determine the permeability of a porous medium, several techniques can be followed: empirical permeability modelling, geometrical permeability models and averaging permeability techniques. The empirical models, in particular, require that several experiments have to be conducted for a range of fibre volume fractions, where Darcy's law is used. Considering the different empirical approaches in the literature, the experimental methods to determine the principal components of the permeability tensor can be classified by [2,11]:

- measurement direction: in-plane or through- thickness;
- type of flow: radial or rectilinear;
- injection type: constant flow rate or constant pressure, and;
- measurement state: transient/unsaturated or steady-state/saturated.

The wide range of permeability measurement techniques reflects the difficulty on the characterization of this property, as minor changes in experimental techniques are reflected as significant discrepancies in the measured values for the same material [4,5,8]. And, despite the importance of accurate permeability characterization for process efficiency, existing methods have not yet been standardized [1,8]. A series of benchmark exercises using in-plane permeability measurement, revealed variations between the participants results as high as 44%, while the average variation of the test for each participant was register as 8% and 12% [8]. It was also showed, however, that by defining minimum requirements for equipment, measurement procedure and analysis, a satisfactory reproducibility of data

can be obtained, even when different systems are used [8]. The differences between results are easily explained by experimental factors, such as [15,16]: cavity deformation, fluid pressure, fluid viscosity, fluid wetting behaviour, reinforcement structure variations, among others [8]. Along with the experimental factors, also, data analysis can affect the final value of permeability [8]. Data deviations are added along the process from data acquisition (by sensors, visual/video monitoring, image analysis, etc.), to the flow front modelling and the analytical approach considered (boundary conditions, simplifications, scaling, etc.).

Compared to linear injection tests, for example, radial injection tests allow by far more variation in these steps, due to the more complex flow front shape and, accordingly, more complex mathematics. To overcome the effect of fluid viscosity variation, Newtonian fluids are usually used in the experiments in order to guarantee there is no change in viscosity with time and/or temperature. Experimental errors are associated to the experimental method, such as: manual fabric cutting and placement, mould deflection, uncontrolled fabric compression, race tracking, errors in the flow position and/or fluid pressure measurements, among others. While the variability of fabric architecture is related to the dual-scale nature of its structures [12]. The internal geometry depends on tow shape and spacing, fibre arrangement and nesting, which, on in turn, vary with draping [17] and compaction, by reduction of thickness, change of porosity pattern and increase in fibre volume fraction [16]. Also, in particular manufacturing processes, such as VARI (Vacuum Assisted Resin Infusion), the internal structure of the fibrous reinforcement changes during the process. For example, impregnation increases the degree of nesting by lubrication. The variations of macroscopic permeability, which is determined in macroscopic flow experiments, can never completely replicate the actual local inhomogeneity. In fact, dual-scale flow effects create differences in overall permeability in the range of 10 to 30% [16].

Considering data analysis to determine permeability, there are four main methods [8]:

- elementary method (applied to the data of each pair of subsequent time steps and calculation of the permeability values based on the differences between the data sets at both time steps. For each pair of subsequent time steps permeability values are obtained which can then be averaged to determine permeability values);
- reference time step method (permeability values are calculated at each time step, considering the difference to the very first time step or another specific time step);
- single step method (permeability is calculated with the data obtained at two particular time steps, e.g., the first and the last);
- global method (calculation is applied to the data of all time steps at once using a fitting procedure).

Thus, permeability values should be considered as a statistical measurement, and a large number of experiments should be performed to precisely measure the statistical parameters and decrease variability and errors [15]. In addition, it also should be measured with a method as close as possible to the manufacturing process.

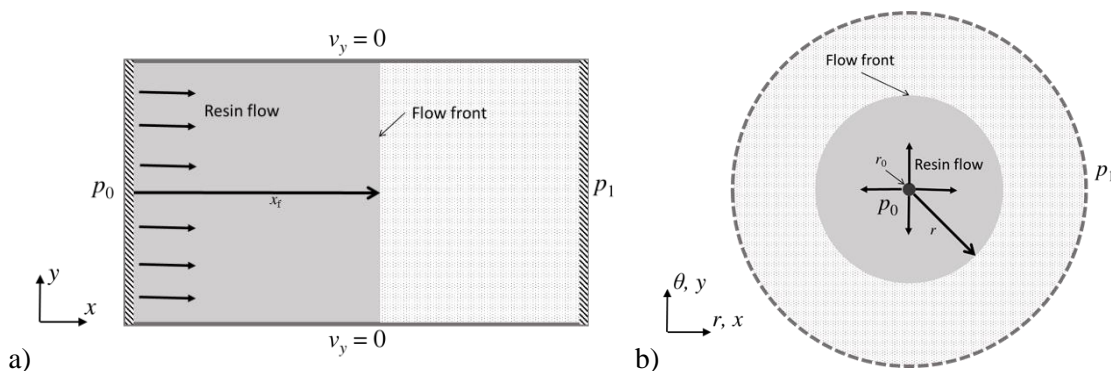


Figure 1: Permeability measurement methods: a) 1D channel flow; b) 2D radial flow.

2.1 In-Plane measurement technique

Weitzenböck et al. [5], differentiated between the channel flow (Figure 1-a) and the radial flow

(Figure 1-b) methods. The channel flow method shows two major disadvantages [1]: race tracking and an experiment is needed for each tensor principal component. In contrast, radial flow experiments allow for a full characterization of the in-plane permeability tensor from a single experiment and avoid race tracking effects, but symmetry of the flow front can be difficult to obtain [1]. Also, due to the more complex flow front shape and, consequently, more complex mathematics, it presents higher variations in data acquisition, flow front modeling and permeability calculation [8].

2.1.1 1D channel/linear Flow method

The linear flow method (Figure 1-a) consists on the injection of fluid through a rectangular shape fibre reinforcement, along a line from one side, and exit on the opposite side also along a line. The flow is assumed to be rectilinear, with zero flow velocity through thickness and side walls (no race tracking). Assuming incompressible Newtonian fluid and a constant pressure gradient, permeability K , is given by Darcy Law along x direction:

$$K = \frac{\mu\phi}{K\Delta p} \frac{x_f^2}{t_f} \quad (4)$$

Equation (4) is applicable to both isotropic and anisotropic materials, but is limited to in-plane permeability tensor principal components.

2.1.2 2D Radial Flow method

In the Radial flow method (Figure 1-b), the resin is injected through a circular centre hole with inlet radius r_0 , in an initially dry preform under constant pressure, and it radiates from the inlet throughout the duration of the experiment. With this method, both in-plane principal components of permeability tensor are determined. For isotropic materials, the flow front is circular with radius r . For simplicity, assuming an isotropic material and a circular inlet, Darcy's Law can be written in cylindrical coordinates as [5,11]:

$$K = \frac{\mu\phi}{4\Delta P} \left(r_f^2 \left[2\ln\left(\frac{r_f}{r_0}\right) + 1 \right] - r_0^2 \right) \frac{1}{t_f} \quad (5)$$

Assuming incompressible Newtonian fluid, the flow occurs only along the plane $r\theta$ (independent of z) and is symmetric around the z -axis (depends only on r), constant pressure gradient, and assuming that the flow front has not reached the walls [5]. For an orthotropic material (Figure 2-a), if the principal direction is unknown (when the principal components of permeability are not coincident to fibre orientation), it is possible to determine the principal permeability values and its direction by determining the permeability in 3 different directions, namely, 0° , 45° and 90° (K_I , K_{II} and K_{III} , respectively), in relation to each other [11].

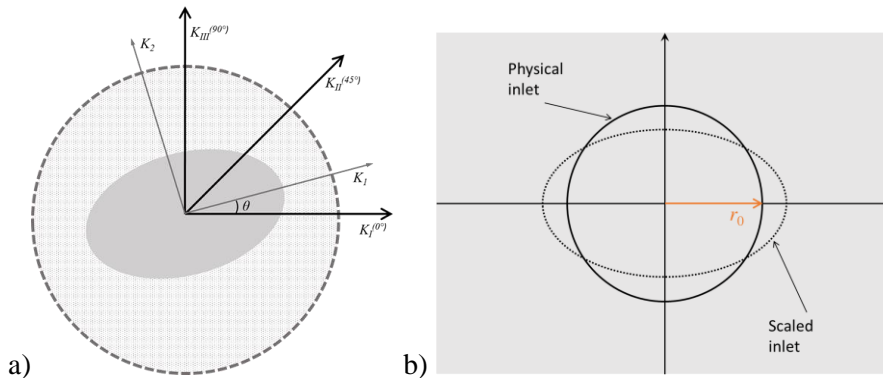


Figure 2: Rotation of the permeability tensor (a). Physical and required inlet dimensions and the elliptic flow front for the fully developed flow, scaling of the circular inlet to an elliptic inlet (b).

Having characterized the reinforcement in three different directions the principal permeability values K_1 and K_2 and the rotation angle θ , can be calculated [5]:

$$K_1 = K_I \frac{(A-D)}{A - \frac{D}{\cos(2\theta)}} \text{ and } K_2 = K_{III} \frac{(A+D)}{A + \frac{D}{\cos(2\theta)}} \quad (6)$$

$$\text{with } \theta = \frac{1}{2} \tan^{-1} \left[\frac{A}{D} - \frac{(A^2 - D^2)}{K_{II} D} \right], A = \frac{K_I + K_{III}}{2} \text{ and } D = \frac{K_I - K_{III}}{2}$$

Also, this approach is valid only for a flow front with similar geometry of the inlet, which is true for isotropic materials, where both inlet and the flow front are circular. However, this is not what it is observed in real experiments, as the inlet is commonly circular while the flow front is elliptic for orthotropic materials. It was already observed experimentally that the flow front eventually develops into an ellipse with constant ratio between the axes, and at some distance away from the inlet it can be assumed the initial shape of the inlet to be elliptic instead of circular [5]. The transformation of the circular inlet into an elliptic one is (Figure 2-b):

$$x_0 = \sqrt[4]{\alpha_1} r_0 \text{ and } y_0 = \sqrt[4]{\frac{1}{\alpha_1}} r_0 \text{ with } \alpha_1 = \left(\frac{x_f}{y_f} \right)^2 = \left(\frac{x_0}{y_0} \right)^2 = \frac{K_1}{K_2} \quad (7)$$

The constant α_1 is a direct measure of the level of anisotropy in the material [8,5]. The closer this ratio is to one, the more circular the flow front is [5].

The effective permeability, which gives the variation of permeability with the rotational angle is expressed as:

$$K_{eff} = \frac{K_1 K_2}{K_1 \sin^2(\theta) + K_2 \cos^2(\theta)} \quad (8)$$

3 EXPERIMENTAL DETERMINATION OF PERMEABILITY

In this study, two different methods were adopted to determine the in-plane permeability tensor components of fibrous reinforcements: 1) linear and 2) radial flows. It is considered that both flows are unsaturated and isothermal, and are driven by constant injection pressure. The compression of the reinforcement is done following two distinct principles: 1) VARI (rigid mould and flexible counter mould) and 2) RTM (rigid mould and counter mould). The test fluid is Newtonian, with constant viscosity, and incompressible. In order to measure permeability, the flow front is monitored through a set of pressure sensors and image analysis. Then the proper analytic relations are applied to obtain the permeability tensor components. The permeability values calculated are then used in the numerical simulation of the impregnation process of thin laminates.

3.1 Materials

3.1.1 Test Fluid

Two different fluids with considerably different viscosities were used (Table 1): glycerine and vegetable oil. Although some researchers pointed out that only in saturated fluid flow, where no capillary effects are present, the type of fluid does not affect the flow (provided that its behaviour is constant during flow) [18], others showed that in unsaturated flow their effect is not significant [19]. The test fluids present Newtonian behaviour along time, at 25°C (Table 1).

Fluid	Dynamic viscosity (mPa.s)	Gel time (min)
Glycerine	1088.6	∞
Vegetable oil	64.5	∞

Table 1: Properties of the test fluids.

3.1.2 Fibrous reinforcements/porous media

Details of the fibrous reinforcement are summarized in Table 2 and Table 3, where properties and structure characteristics are listed, respectively. The selected fibrous reinforcement (X450), is a biaxial

non-crimp structure, stitched.

Type of fibre	Structure	Total Areal weight (g/m ²)	Areal weight 0° (g/m ²)	Areal weight +45°/-45° (g/m ²)	Areal weight 90° (g/m ²)	Stitching yarn (g/m ²)	Thickness (mm)
X450 Glass	Non crimp biaxial ±45° (stitched)	444	1	217	1	5	0.542

Table 2: Characteristics of the fibrous reinforcement X450.

X450	
Structure	
Construction warp (bundles/cm)	5
Construction weft (bundles/cm)	5
Stitches width (mm)	0.1
Stitches distance (mm)	5
Bundle/warp width (mm)	2.0
Bundle/weft width (mm)	2.0

Table 3: Structure characteristic of fibrous reinforcement.

3.2 Methods

As stated previously, four different methods are considered: linear and radial flow following the principles of VARI and RTM manufacturing processes. In other words, it is considered different resin inlet (point in the centre of the sample, for radial flow, and line along the total length of the sample, for linear flow), type of compression exerted on the fibre reinforcement (flexible and rigid mould compression for VARI and RTM principles, respectively) and different influx of fluid (injection for the RTM principle and suction for the VARI principle).

The sample preparation was done avoiding unnecessary handling, to prevent distortions of the structures. The reinforcement layers were cut out (following the rule that 0° corresponds the production direction) and stacked at identical orientation. In the particular case of radial flow tests, an inlet hole (with 8 mm diameter), was punched on the complete stacks, guaranteeing that the flow is done only along the in-plane. The weight of the samples is registered.

The test is done by placing a dry sample of fibrous reinforcements on top of the bottom rigid plate. Then the fibrous reinforcement is compressed by a flexible (VARI) or rigid (RTM) counter mould that seals the system. The final thickness of the compressed reinforcement is registered. Finally, the fluid is injected from the inlet into the system using constant pressure gradient, and the flow progresses along the sample up to the outlet. The flow progression is recorded in real time, by image analysis (in the VARI method) and pressure sensors (in the RTM method), in order to obtain the time necessary for the flow front to travel specific distance. From the data obtained, the permeability of the reinforcement can be calculated. The tests were performed at least 3 times for each case.

For the flow data analysis, different methodologies are considered. The main one is the global method, which is based on the best line fit and considers all data, and the work of Weitzenböck [5] is used as reference. Other methodologies are inlet scaling (x_0 and y_0) and exclusion of the initial flow data. In the former methodology, equation (7) is applied (Figure 2-b). In the later, permeability is determined

by excluding the data of the first few centimeters from the inlet, where transient effects are originated by the sudden sharp drop of the applied liquid pressure when the valve is opened and the rapid recovery of the pressure occurs. In this case, the permeability is determined in each time step and the average is calculated from the period of time where the permeability is relatively constant.

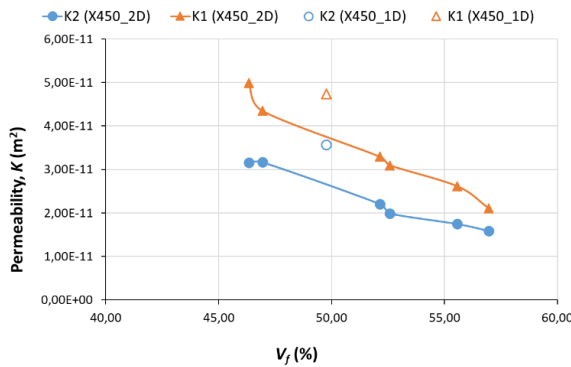
3.3 Permeability

Both linear and radial test methods were used to determine the in-plane permeability tensor components. In this first approach, tests were performed following the guidelines proposed in [8], in order to directly compare the results. In addition, the reinforcement was also tested using linear flow. While the radial tests were done for different fibre volume content, V_f , (Figure 3) as in [], the linear test was only done for one V_f value. Table 4 summarizes the test conditions considered.

Reference	Type of flow	Type of compression	Type of fluid	Number of layers	ΔP (bar)
X450_2D	radial	RTM	Glycerine	6	2.038±0.032
X450_1D	linear				
X450_2D-V	radial	VARI	Vegetable oil		0.988±0.002
X450_1D-V	linear				

Table 4: Test conditions.

Figure 3 shows a consistent decrease of permeability values with increasing V_f , as expected, as well as K_1 is consistently higher than K_2 . However, the permeability tensor determined by linear flow method leads to significantly higher permeability values.



Ref.	V_f (%)	K_1 (m ²)	K_2 (m ²)
X450_2D	46.34	4,991E-11	3,159E-11
	46.94	4,348E-11	3,166E-11
	52.13	3,295E-11	2,207E-11
	52.57	3,099E-11	1,990E-11
	55.57	2,614E-11	1,745E-11
	56.95	2,108E-11	1,587E-11
X450_1D	49.77	3,564E-11	4,738E-11

Figure 3: Permeability (K) variation with fibre volume content (V_f) for reinforcement X450, using RTM principle for radial and linear flow.

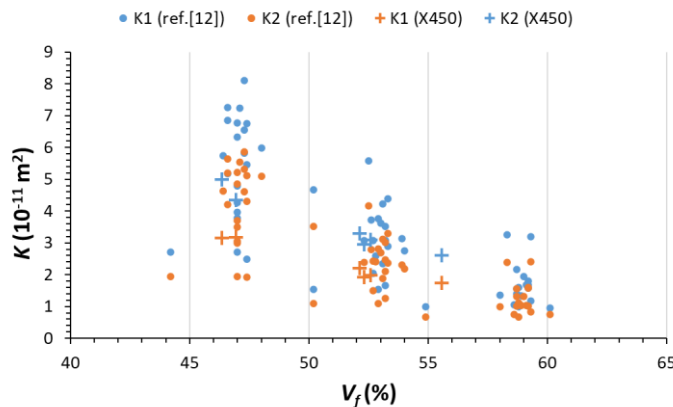


Figure 4: Variation of K_1 and K_2 with the fibre volume fraction (V_f): comparison with the results of reference [8].

The X450 structure is almost exactly the same as the biaxial structure used in the benchmark study [8], so, the results obtained in this work are compared directly to those published by [8], in Figure 4. The obtained experimental results are within the variation range. However, looking to all the results, the differences could be as higher as 40%. Figure 4 clearly depicts the high scattering of the determined permeability values.

The in-plane permeabilities of the reinforcement X450 (Table 5) were also determined by the test method following VARI principle (Table 4). This set of tests were used to either compare the permeability values with the RTM test method and compare the permeability values obtained with different calculation approaches. Comparing the permeability values from Figure 3 and Table 4, the RTM principle test, independently of the flow type, gives higher permeability values.

Ref.	V_f (%)	Experimental			Principal components		
		K_I (m ²)	K_{II} (m ²)	K_{III} (m ²)	θ (°)	K_1 (m ²)	K_2 (m ²)
X450_2D-V	55.49	8.813	8.097	6.186	15.13	9.119	6.044
X450_1D-V	55.05	6.140	5.641	3.569	18.52	6.754	3.390

Table 5: Permeability values (given as E-12) for VARI principle method with radial and linear flow.

Thus, following the calculation method of permeability proposed by Weitzenböck [5], previously described, K_I , K_{II} and K_{III} (Table 5) are determined in both radial and linear methods using the experimental data obtained from the monitoring of the flow front. The orientation of these three permeabilities is assumed to be the production orientation, i.e., K_I is oriented 0°, while K_{II} and K_{III} are oriented 45° and 90°, respectively. Is important to note, however, that in the production direction the fibres are oriented at $\pm 45^\circ$. The principal components of the permeability tensor (K_1 and K_2) are, then, calculated using the set of expressions in equation (6). Table 5 shows that the permeability tensor and, consequently, the in-plane permeability components, are rotated by 15.13° relative to production direction, and 29.87° relative to fibre direction.

If other considerations are taken in account in the data analysis, such as scaling, excluding the initial data, and the average of the constant permeability, as suggested, for example, in [5], [18] and [20], and described previously, the in-plane permeability tensor components can be recalculated. These permeability values are summarized in Table 6. The results show that, for the same experimental data, significant differences are obtain depending on the data analysis method in both permeability values and permeability angle (θ). Comparing to the original permeability values and angle (Table 5), scaling slightly alters these values (Table 6). Averaging results in a small increase in the permeability values, but significantly decreases the permeability angle, while, excluding the initial experimental data results in a considerable decrease in both permeability and rotational angle values (Table 6). The overall differences on the variation of permeability with the rotational angle are depicted in Figure 5, where the effective permeability (K_{eff}), for the permeability values obtained by the different data analysis methods, is plotted (where K_{eff_2D} is the effective permeability for the original permeability principal components in Table 5). K_{eff} is calculated using equation (8). Figure 5 shows that by excluding the initial experimental data leads to a significant different permeability tensor.

Ref.	θ (°)	Scaling		θ (°)	Data excluded		θ (°)	Average	
		K_1 (m ²)	K_2 (m ²)		K_1 (m ²)	K_2 (m ²)		K_1 (m ²)	K_2 (m ²)
X450_2D-V	16.11	8.965	6.145	-1.99	6.646	3.899	6.46	9.165	6.445

Table 6: permeability values for VARI method. Permeability values are gives as E-12 (m²).

The same analysis was done using linear flow test method (X450_1D-V), with test condition in Table 4, and experimental and principal components of the permeability tensor in Table 5. Figure 5 and Table 5 show that the permeability tensor obtained from the linear flow test method (K_{eff_1D}) is considerably different form the permeability tensor obtained from the radial flow test method (K_{eff_2D}). The same result was observed for the test method following the RTM principle (Figure 3). Curiously, the permeability tensor K_{eff_1D} is similar to the permeability tensor obtained by the data analysis that

excludes the initial experimental data.

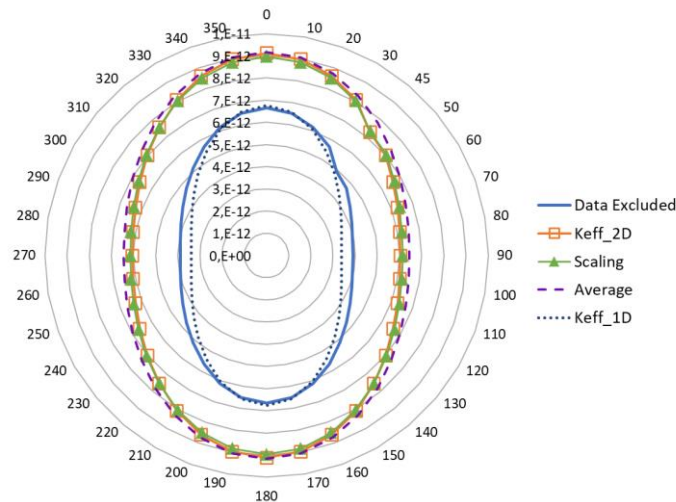


Figure 5: Variation of effective permeability (K_{eff}) with rotational angle (θ), for the different permeability tensors.

4 FLOW FRONT SIMULATION

Since the permeability tensor is the main property to be defined for the reinforcement material, it is important to feed the numerical model with accurate values. As showed in the previous section and by several benchmark studies [8-10], the determination of the permeability tensor depends on several factors, such as: test method (type of flow, state, handling of the reinforcement, etc.) and data analysis. With this, the following question arises: which method and data analysis is the best? Many published investigations show good correlation between numerical and experimental results, considering permeability tensor obtain from the most varied test methods [8-10], suggesting, possibly, that it is the combination of the best test method for the specific numerical approach that results in accurate correlations. Thus, this approach will allow us to evaluate which experimental method and data analysis provide the best permeability tensor to be applied in the simulation, so that the numerical results accurately mimic the experimental data.

PAM-RTM finite element software, by ESI, was used to simulate the flow front progression. Both linear and radial flows are simulated considering, in the numerical models, the experimental test conditions described in the previous sections as inputs, in order to compare directly to the experimental flow front data. The schemes of the linear and radial simulation models are illustrated in Figure 6. The simulation model was built considering a rectangular and circular shape preform for the linear and radial flows, respectively (Figure 6). The mesh was assembled using shell tetra elements, as the focus of the study is the in-plane flow, and the out-of-plane flow can be neglected for thin reinforcements. The boundary conditions were defined on the model exactly as in the experimental impregnation process, and described in Table 4.

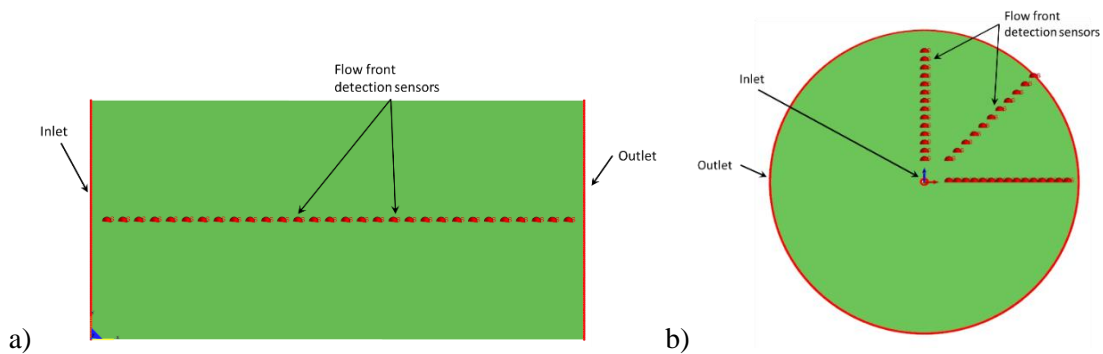


Figure 6: Scheme of the numerical model, for the simulation of the impregnation process for: a) linear test method and b) radial test method (from Figure 1).

4.1 Linear flow permeability

The flow front progression obtained from the simulation of the linear flow, considering the permeability tensor determined by the linear flow test method X450_1D-V (Table 5), is compared with the experimental data obtained by the same method in Figure 7. Both numerical and experimental data were extracted from the central line of the preform. The graphic shows very good correlation for both in-plane principal components of the permeability tensor (Figure 7-a). In the same graphic, the flow front progression using the permeability tensor calculated using radial flow test method (X450_2D-V from Table 5) in the numerical model, is also plotted and compared. As expected, due to the considerably different permeability distribution (Figure 5), no correlation is obtained. These results are confirmed by Figure 7-b, where the overall experimental and numerical flow front are superimposed. It also shows the significant effect of the race tracking effect, which is not reproduced by the simulation.

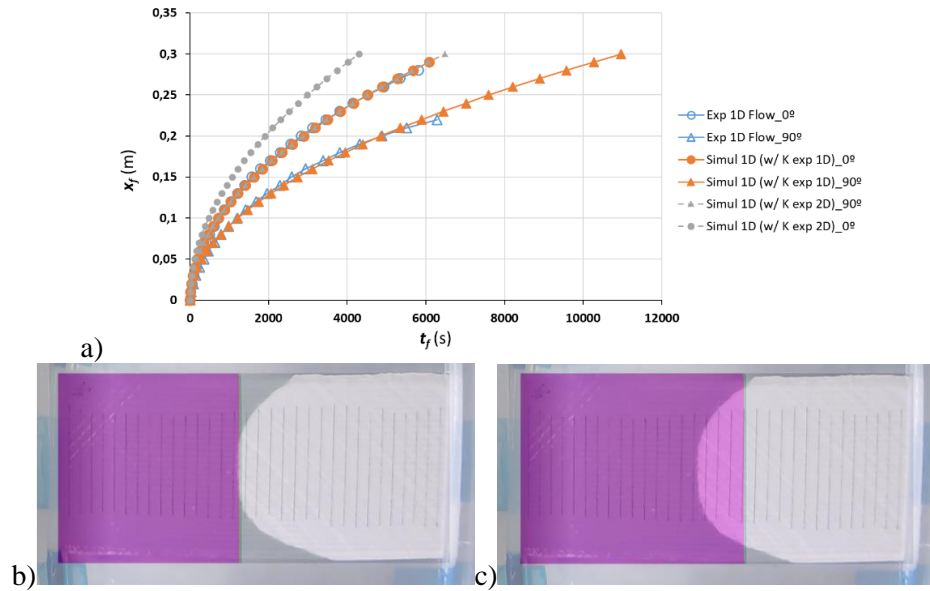


Figure 7: Linear flow test. Comparison of the experimental and numerical results: a) extracted from the central line; and general view of the flow front at 90°, at $t_f = 1500$ s, with permeability tensor determined by b) linear and c) radial flow.

4.2 Radial flow permeability

Using the different permeability values, calculated and presented in Table 5 and Table 6, as inputs, the flow front progression of radial flow were compared with the experimental data, including the permeability tensor determined through the linear flow test method. These results are summarized in Figure 8. In general, the difference between the numerical and experimental results increases with the distance from the inlet. However, the permeability tensor determined by the initial data excluded approach and the linear flow test present the best correlation with the experimental results considering 0° direction (Figure 8-a), while for 45° (Figure 8-b) and 90° (Figure 8-c) every approach present similar discrepancy for upper or lower values. Average, scaling and original permeability tensor have faster flow front progression than the experimental. Instead, data excluded approach and the permeability tensor determined by linear flow present slower flow front progression.

Looking to the total in-plane flow front progression at $t_f = 2100$ s, for example, the overlapping of numerical and experimental results is illustrated in Figure 9. The results also show that the experimental flow front is not symmetric. This is a problem for permeability measurement, because depending on the circle quadrant chosen to be analyzed different results will be obtained. However, it confirms that the approach where the initial data are excluded and the permeability tensor obtained by linear flow method present the best correlation with experimental results.

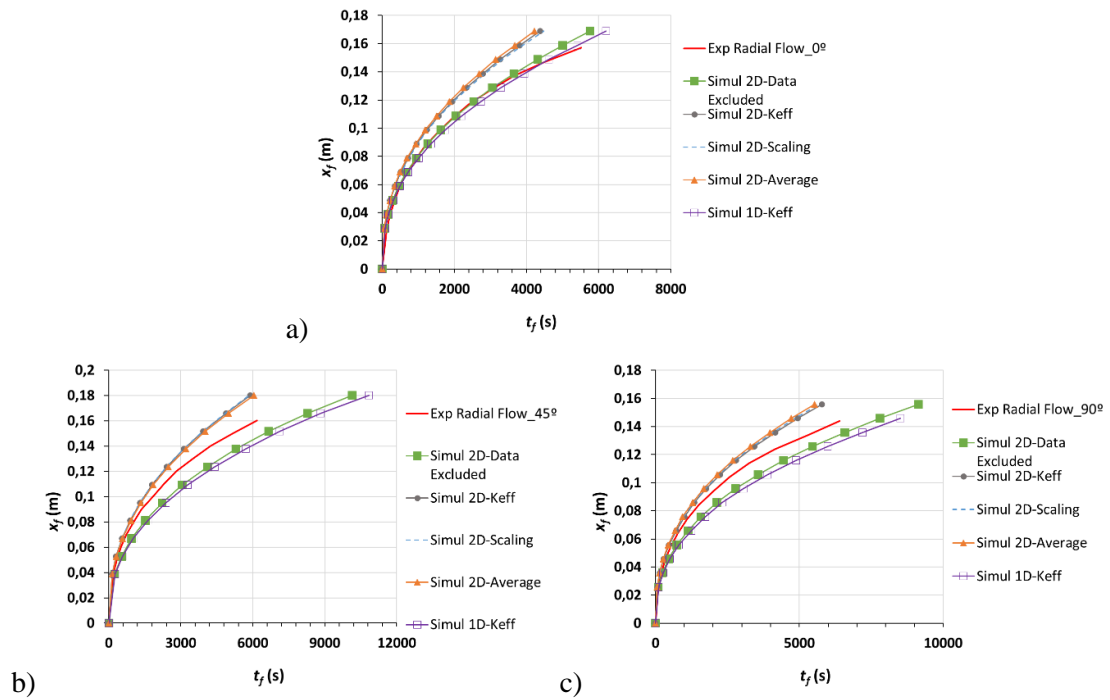


Figure 8: Flow progression of the radial flow test: comparison of the experimental and numerical results at direction a) 0°, b) 45° and c) 90°.

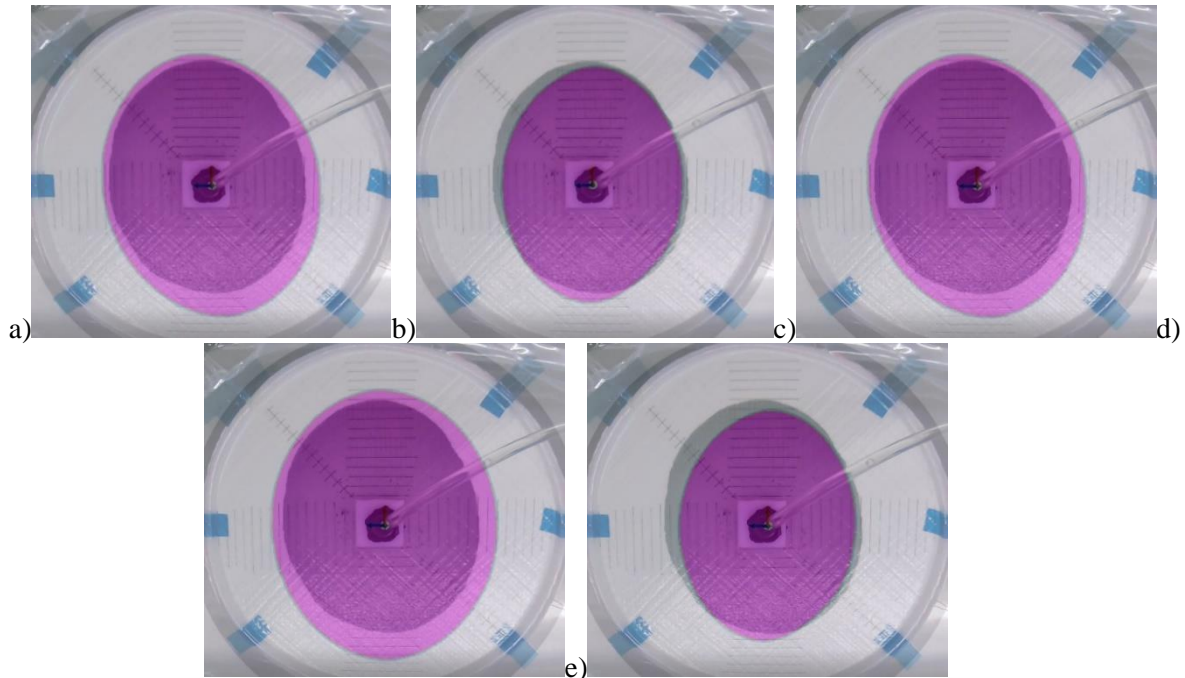


Figure 9: Flow progression of the radial flow test: comparison of the experimental and numerical results: a) 2D original permeability; b) initial data excluded; c) scaling; d) averaging; e) 1D permeability.

5 CONCLUSIONS

In this work, different experimental methods and data analysis approaches were used in order to determine which provides the permeability tensor that can be correlated to numerical simulation using PAM-RTM. As the obtained values of the permeability tensor principal components depend on several factors, and in the absence of a standard procedure to follow, the best path is the one that suits better the

numerical analysis in use. Our results show that, the determination of permeability by linear flow and by radial flow with the initial data excluded from calculations, present the best correlation between experimental and numerical results. However, caution is needed in extrapolating these conclusions, since the same may not be applied to other reinforcement structures or complex geometries, which should be verified in future work.

REFERENCES

- [1] Fauster E, et al. Image processing and data evaluation algorithms for reproducible optical in-plane permeability characterization by radial flow experiments. *J Compos Mater* **53**(1), 2019, pp.45-63.
- [2] Zénone CI, Le Grogne P, Park CH. Characterization and modeling of composite Vacuum Infusion process: Influence of fabric type, resin viscosity and strain rate. *IOP Conf Ser Mater Sci Eng.* 2018;406(1). doi:10.1088/1757-899X/406/1/012062
- [3] Dullien FAL. Porous Media: Fluid Transport and Pore Structure. 1979.
- [4] Koefoed MS. Modeling and Simulation of the VARTM Process for Wind Turbine Blades. PhD Diss. 2003, Aalborg University.
- [5] Weitzenböck, J. R. (1996). Flow Characterisation in Resin Transfer Molding. Ph. D. thesis, Southampton University.
- [6] Caccia M, et al. Wetting and Navier-Stokes equation – the manufacture of composite materials. In: Aliofkhaezrai M (ed.) *Wetting and wettability*. London, UK: IntechOpen Limited, 2015.
- [7] Lu S, et al. Real-time monitoring of resin infiltration process in vacuum assisted molding (VARI) of composites with carbon nanotube buckypaper sensor. *Mater Res Express.* **6**(115628), 2019, pp.1-12.
- [8] May D, et al. In-plane permeability characterization of engineering textiles based on radial flow experiments: A benchmark exercise. *Compos Part A Appl Sci Manuf.* **121**, 2019, pp.100-114.
- [9] R. Arbter, et al. Experimental determination of the permeability of textiles: a benchmark exercise. *Compos A Appl Sci Manuf*, **42**(9), 2011, pp.1157–68.
- [10] N. Vernet, et al. Experimental determination of the permeability of engineering textiles: benchmark II. *Compos A Appl Sci Manuf*, **61**, 2014, pp.172–84.
- [11] Adams KL, Russel W and Rebenfeld L. Radial penetration of a viscous liquid into a planar anisotropic porous medium. *Int J Multiphase Flow* **14**, 1988, pp. 203–215.
- [12] Ali, M. A., et al. In-plane virtual permeability characterization of 3D woven fabrics using a hybrid experimental and numerical approach. *Composites Science and Technology*, **173**, 2019, pp.99–109.
- [13] Yun M, Sas H, Simacek P, Advani SG. Characterization of 3D fabric permeability with skew terms. *Compos Part A Appl Sci Manuf.*, **97**, 2017, pp.51-59.
- [14] K. Okonkwo, P. Simacek, S.G. Advani, R.S. Parnas. Characterization of 3D fiber preform permeability tensor in radial flow using an inverse algorithm based on sensors and simulation. *Composites: Part A*, **42**, 2011, pp.1283–1292.
- [15] Michaud, V. Permeability properties of reinforcements in composites. In P. Boisse (Ed.), *Composite Reinforcements for Optimum Performance* (1st ed.). Woodhead Publishing Limited.
- [16] Bodaghi, M., et al. On the variability of permeability induced by reinforcement distortions and dual scale flow in liquid composite moulding: A review. *Composites Part A: Applied Science and Manufacturing*, **120**, 2019, pp.188–210.
- [17] Pierce, R. S., Falzon, B. G., & Thompson, M. C. Permeability characterization of sheared carbon fiber textile preform. *Polymer Composites*, **39**(7), 2018, pp.2287–2298.
- [18] Staal, J., et al. In-series sample methodology for permeability characterization demonstrated on carbon nanotube-grafted alumina textiles. *Composites Part A: Applied Science and Manufacturing*, **150** (106631), 2021, pp.1-11.
- [19] Luo, Y., et al. Permeability measurement of textile reinforcements with several test fluids. *Composites - Part A: Applied Science and Manufacturing*, **32**(10), 2021, pp.1497–1504.
- [20] Elinor Swery, et al. Efficient experimental characterisation of the permeability of fibrous textiles. *Journal of Composite Materials*, **50** (28), 2016, pp.4023-4038.